A dimensional comparison between embedded 3D-printed and silicon microchannels

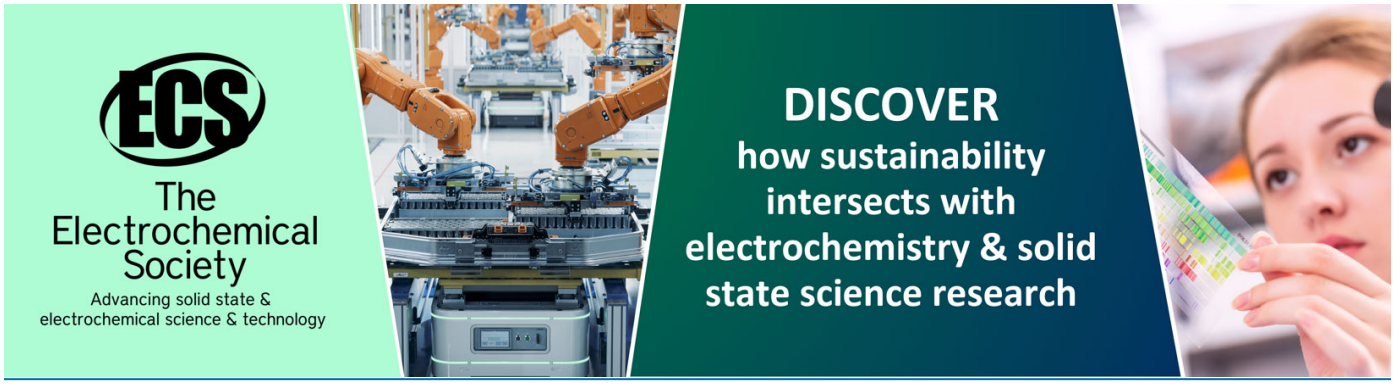

Journal of Physics: Conference Series **525** (2014) 012009 doi:10.1088/1742-6596/525/1/012009

A dimensional comparison between embedded 3D-printed and silicon microchannels

J O'Connor[1], J Punch[1], N Jeffers[2] and J Stafford[2]

[1] CTVR, Stokes Institute, University of Limerick, Limerick, Ireland
[2] Thermal Management Research Group, Bell Labs Ireland, Alcatel-Lucent, Blanchardstown, Co. Dublin, Ireland

E-mail: john.patrick.oconnor@ul.ie

Abstract. The subject of this paper is the dimensional characterization of embedded microchannel arrays created using contemporary 3D-printing fabrication techniques. Conventional microchannel arrays, fabricated using deep reactive ion etching techniques (DRIE) and wet-etching (KOH), are used as a benchmark for comparison. Rectangular and trapezoidal cross-sectional shapes were investigated. The channel arrays were 3D-printed in vertical and horizontal directions, to examine the influence of print orientation on channel characteristics. The 3D-printed channels were benchmarked against Silicon channels in terms of the following dimensional characteristics: cross-sectional area (CSA), perimeter, and surface profiles. The 3D-printed microchannel arrays demonstrated variances in CSA of 6.6-20 % with the vertical printing approach yielding greater dimensional conformity than the horizontal approach. The measured CSA and perimeter of the vertical channels were smaller than the nominal dimensions, while the horizontal channels were larger in both CSA and perimeter due to additional side-wall roughness present throughout the channel length. This side-wall roughness caused significant shape distortion. Surface profile measurements revealed that the base wall roughness was approximately the resolution of current 3D-printers. A spatial periodicity was found along the channel length which appeared at different frequencies for each channel array. This paper concludes that vertical 3D-printing is superior to the horizontal printing approach, in terms of both dimensional fidelity and shape conformity and can be applied in microfluidic device applications.

1. Introduction

Industry has benefited greatly from the introduction of microfluidic technologies including thermal management, biotechnology, and health care. As an example, thermal management has seen improved heat flux dissipation from increasingly smaller areas which serves in maintaining chip temperature and reducing localised hot spots in integrated circuit devices [1]. When developing microfluidic devices or structures, a number of different channel manufacturing techniques exist for both thermal management and Lab-on-a-chip(LOC) applications. For thermal management applications, chemical etching of Silicon wafers using deep reactive ion etching (DRIE) or wet-etching techniques (KOH) is the conventional method of channel fabrication. Anodic bonding is then used to create a permanent seal between a glass slide and the Silicon wafer [2]. In LOC applications, Polydimethlysiloxane (PDMS) or Poly(methyl methacrylate) (PMMA), casted from a Silicon mold, is the conventional method of microchannel fabrication and was initially demonstrated by Martynova *et al.*[3]. The channels are sealed by bonding the microchannel to a glass slide using PDMS or some other Silicone based polymer. Although it can be important to have dimensionally accurate and uniform channels, there are

limitations associated with these methods of manufacture: primarily cost, flexibility of design, and fabrication time. Rapid-prototyping, in particular 3D-printing, is a cost-effective and swift alternative.

Rapid-prototyping is the fabrication of a structure or assembly using computer aided design files in a stereo-lithography file format. Specifically, the type of rapid-prototyping under investigation in this paper is 3D-printing. Modern commercially-available 3D-printers are capable of printing to a resolution of 16 μm with a range of polymeric materials. Typically, the 3D-printing process involves depositing a sacrificial base layer followed by the print material and in areas where there is an embedded or overhanging feature, sacrificial material is deposited to maintain the parts' structure. High layer resolution and flexible design offered by commercial 3D-printers facilitates the creation of embedded microchannels within structures, provided there is a method to expel the sacrificial material from the embedded feature. Microfluidic studies using 3D-printing as an alternative to conventional techniques are becoming more commonplace in the literature and the following paragraph details studies which use 3D-printing in microfluidic research.

Payder *et al.* [4] designed and characterized 3D-printed microfluidic interconnects integrated with an O-ring. This device provided an effective interconnection, as it could sustain pressures exceeding 400kPa with no leaks. McDonald *et al.* [5] investigated 3D-printed molds as an alternative to Silicon molds for casting PDMS microchannels. It was found that channel quality increased at higher resolutions, and that surface roughness was measured to be 10-20 μm with no periodic patterning evident along the channels. Moore *et al.* [6] detailed the cost effectiveness and the fast fabrication times of 3D-printing, and used this method to evaluate a passive valve design for a centrifugal LOC disk. This work characterized the surface profile of the 3D-printed part and revealed a high degree of spatial periodicity across the top surface, while the microchannel structure printed had a distorted base with clear passive valve features present at the side-wall. Bonyár *et al.* [7] reported similar findings, whereby molds were 3D-printed for PDMS casting. This work also investigated 3D-printed LOC structures which were sealed using an adhesive film. Krejcova *et al.* [8] used a similar methodology to fabricate a chip which was developed as a virus detection system. Finally, McCullough and Yadavalli [9] investigated the suitability of poly(acrylonitrile butadiene styrene) for 3D-printed biomedical device fabrication using fusion deposition modelling; this involved surface treatment and surface characterization of the microchannel. The surface modifications created bio-compatible, hydrophilic, and water impermeable microchannels.

The studies described here use 3D-printing techniques which created troughs on a single plane of material. It is also important to note that no studies exist that characterize embedded 3D-printed channels. The aim of this paper is the characterization of these 3D-printed embedded microchannel arrays. This paper will discuss the objectives, methodologies used to characterize the channels, and measured dimensional characteristics of the microchannels. It paper concludes with the findings of the dimensional characterization and a summary of the implication for microchannel fabrication via 3D-printing.

2. Objectives

The overall objective of this paper is the dimensional characterization of embedded microchannel arrays. To this end, the specific objectives are as follows:

- To compare the twenty-two channel DRIE and KOH Silicon microchannel arrays characterized by Eason *et al.* [2] with an equivalent 3D-printed design using vertical and horizontal 3D-printed techniques. The dimensions of the channel geometries are illustrated in figure 1.
- To evaluate the performance of both vertical and horizontal 3D-printing techniques with regard to fabricating embedded microchannel arrays. A total of twelve microchannel arrays

were investigated; a statistical sample of three was taken for each shape and these shapes were printed in both orientations.

- To characterize 3D-printed microchannel arrays geometrically by measuring cross-sectional area (CSA), perimeter, aspect ratio and surface profiles in order to quantify the dimensional fidelity and precision of 3D-printed microchannels.

3. Methodology

This section describes the fabrication process for both the vertical and horizontal 3D-printed microchannel arrays and details how these arrays were prepared after printing. The dimensional characterization procedures for both cross-sectioning and surface profiling are described.

3.1. Manufacture

The 3D-printed microchannel arrays characterized in this paper were created using a Projet HD 3500 3D-printer at its highest resolution setting. The highest achievable layer resolution, as stated by the manufacturer, was 16 μm in the x, y, and z directions. The materials used to create the microchannel arrays were Acrylonitrile as the 3D-printing material and wax as the sacrificial material. Two different printing orientations were explored to examine the influence of print direction on channel characteristics: vertical and horizontal 3D-printing approaches, as illustrated in figure 2.

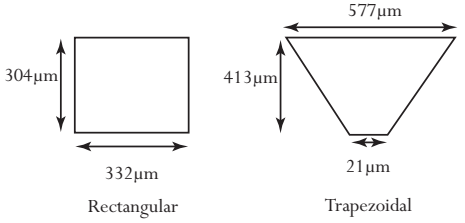

Figure 1. Nominal channel shapes and dimensions.

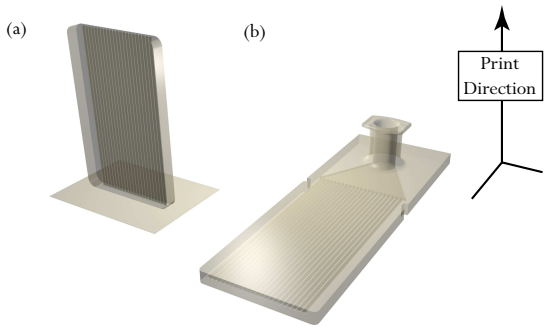

Figure 2. Perspective view of embedded channel designs, (a) vertical and (b) horizontal, which is representative of their orientation in the 3D-printer.

Vertically printing the channels ensured that only 3D-printed material formed the channels with no wax occupying the channels. Horizontally printing the channels, involved filling the channel with the support material, wax. To clean the horizontal channels, the arrays were then heated to 57°C in a oil bath to melt the wax within the embedded features. It was evident that wax melted when the channels were optically transparent. The channels were flushed out several times with syringes containing clean hot oil free from contaminants, hot water mixed with detergent and clean water. This process was repeated several times, as the presence of any remaining wax, oil or detergent would be diminished every time the process was repeated.

3.2. Channel measurement

The samples were cross-sectioned with a dicing saw and potted in epoxy. Samples were aligned perpendicular to the pot base to ensure a true cross-section of the channel (<1°). The epoxy encasing each sample was polished to a mirror finish and images of every channel were taken using a Hitachi TM1000 Tabletop Scanning Electron Microscope (SEM). The polished cross-sections were sputtered with a submicron layer of gold to eliminate charging while in the SEM. A custom MATLAB routine was used to measure area, perimeter, width, and height

of each cross-section. To minimize uncertainty in channel measurement, the scale bar was calibrated to pixel length to a resolution of 0.52 and 0.69 μm per pixel for 200 and 300 μm scale bars respectively. A representative polygon of the cross-section was taken, by selecting a series of points along the cross-section. The number of points selected was varied with shape complexity, with a minimum of 200 points taken for each image. A sensitivity analysis showed that a minimum of 200 points was needed to measure the channel area to within 0.9 %. A custom function was used to calculate area, and the sum of the length between points was used to calculate perimeter. Characteristic heights and widths were measured using the scaled images. This measurement methodology was similar to that of Eason *et al.* [2].

Channel length profile measurements were taken with a Hommel T500 surface profilometer to investigate the variance in channel wall roughness and, subsequently, CSA variance in the lengthwise direction. The samples were precision machined to expose the area of interest. The profile probe measured a length of 4.8 mm with the horizontal and vertical resolution of the scan was 2.4 μm and 0.02 μm respectively. The probe tip diameter was 2 μm. Each measurement was repeated three times to ensure that no damage was done to the channel and a consistent reading was taken.

4. Dimensional characteristics

This section discusses the CSA, channel dimensions and profilometry measurements for the vertical and horizontal 3D-printed microchannel arrays. CSA measurements for both Silicon microchannel arrays were also reported.

4.1. Vertical channels

Figure 3 depicts typical cross-sections of the rectangular and trapezoidal vertical 3D-printed microchannel arrays. The rectangular cross-section shows good shape conformity, with curvature present at the corner and base wall. This cross-section is similar to conventional DRIE microchannel cross-section, as shown by other authors [2][10]. The trapezoidal cross-section shows good shape conformity, with curvatures present at all corners and a base width larger than the nominal. The reason for the curvatures and larger base width is due to material shrinkage during the printing process [11].

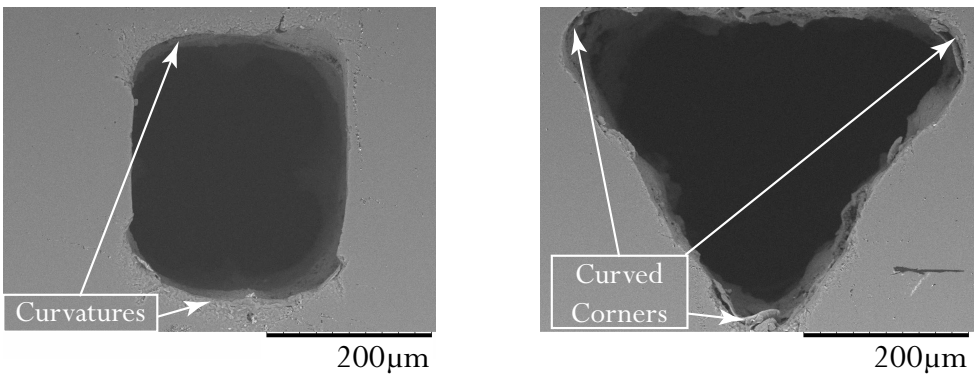

(a) Rectangular (b) Trapezoidal

Figure 3. Cross-sections of the vertical 3D-printed microchannel array shapes:(a) Rectangular, and (b)Trapezoidal.

Table 1 contains the measured average CSA and perimeter, the channel–to–channel variance and deviation from the nominal dimensions for each microchannel array.

[1] The labelling system describing each 3D-printed channel examined here, are labelled in terms of shape, orientation and number in sample size. The letters used are explained as follows: R = rectangular, T = trapezoidal,

Table 1. Comparison of the nominal and measured CSAs (mm^2),and perimeter (mm)for the vertical 3D-printed channels. Channel-to-channel variance per array and percentage deviation from the nominal dimension are presented.

Channel Type [1]	Nominal		Measured		Variance (%)		Change (%)	
	CSA	Perimeter	CSA	Perimeter	CSA	Perimeter	CSA	Perimeter
DRIE	0.101	1.27	0.099	1.20	2.7	2.1	-2.3	-0.1
KOH	0.123	1.50	0.117	1.50	4.9	4.3	-4.96	-5.8
RV1	0.101	1.20	0.087	1.10	7.7	4.9	-13.9	-8.3
RV2	0.101	1.20	0.086	1.10	10.2	6.8	-14.5	-8.4
RV3	0.101	1.20	0.097	1.20	11.7	4.5	-3.7	-0.5
TV1	0.123	1.50	0.115	1.40	7.5	6.6	-6.5	-6.6
TV2	0.123	1.50	0.115	1.41	6.0	4.6	-6.6	-6.0
TV3	0.123	1.50	0.104	1.31	9.0	5.1	-16.2	-12.6

All CSAs for both the rectangular and trapezoidal microchannel arrays were less than the nominal dimensions of the Silicon channels (-3.7– -16.2 %) with deviating channel-to-channel variances of 6.0–11.7 %. The perimeter measurements were less than the nominal dimensions; this is due to the curvature features present at the corners of each shape which reduce the perimeter. These deviations have been documented in other studies [5]. A possible reason for these deviations would be the effect of printer resolution, combined with material shrinkage associated with 3D-printing, which is a non-linear and a highly sensitive parameter [11]. In comparison to the Silicon channels, the variances associated with area and perimeter were 2.7 and 2.1 % for DRIE and 4.9 and 4.3 % for KOH, which are comparable to the 3D-printed channels.

Table 2 presents a comparison of the measured channel dimensions against the nominal, with associated deviations from nominal and variances of both dimensions.

Table 2. Comparison of the nominal and measured channel dimensions for the vertical 3D-printed channels. Channel-to-channel variance per array and percentage deviation from the nominal dimensions are presented.

Channel Type	Nominal (mm)		Measured (mm)		Change (%)		Variance (%)	
	Height	Width	Height	Width	Height	Width	Height	Width
DRIE	0.304	0.332	0.304	0.332	n/a	n/a	n/a	n/a
KOH	0.413	0.577	0.413	0.577	n/a	n/a	n/a	n/a
RV1	0.304	0.332	0.319	0.284	5.0	-14.4	5.3	6.6
RV2	0.304	0.332	0.314	0.300	3.2	-9.6	8.4	5.6
RV3	0.304	0.332	0.357	0.310	17.4	-6.5	7.8	10.8
TV1	0.413	0.577	0.362	0.456	-12.3	-20.9	7.3	7.7
TV2	0.413	0.577	0.382	0.479	-7.4	-16.9	2.9	5.6
TV3	0.413	0.577	0.363	0.442	-12.1	-23.4	7.1	7.6

The measured channel height fluctuated about the nominal (-12.3–17.4 %), while the channel widths were consistently smaller than the nominal. Reasons for such variance in the channel

V = vertical, H = horizontal. This labelling system will be used in all tables in this paper.

dimensions are due to both limited resolution and material shrinkage reducing both sharp corner features.

Vertical printing does vary in dimension and deviates from the nominal in both cases studied, however the variances range between two to four times larger than that of conventional Silicon fabrication. Other effects, such as shrinkage and resolution, should be accounted for in the design stage, as decreasing scale will result in larger variance. Although vertical printing is limited by its design flexibility, it does provide a swift and relatively cheap fabrication solution.

4.2. Horizontal channels

Figure 4 shows sample cross-sections for each horizontal 3D-printed microchannel array. A notable and common feature shared by both channels is the inherent roughness present at the side-walls. The rectangular channel cross-section, figure 4(a), has a rectangular profile, but the side-wall roughness distorts the channel shape. The trapezoidal cross-section, figure 4(b), shows a highly distorted trapezoidal shape. The side-wall roughness is more pronounced than the rectangular cross-section and, as a result, the base width dimension is not visible. There is an arching feature present at the top of the trapezoidal cross-section which reduces the sharp corner of the nominal shape. It is difficult to pinpoint this side-wall roughness feature origin; however one explanation would be an interaction between both the wax and 3D-printer material while being printed layer by layer during fabrication.

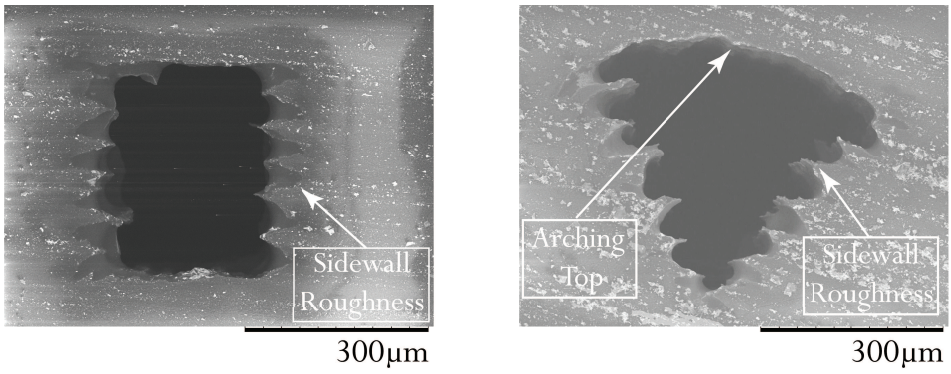

(a) Rectangular (b) Trapezoidal

Figure 4. Cross-sections of the horizontal 3D-printed microchannel array shapes (a) rectangular and (b) trapezoidal.

Table 3 details the measured CSA and perimeter of each microchannel array, with the variance and deviation from the nominal.

A large variance in CSA and deviation from the nominal exists for both horizontal printed shapes (-31.7–41.9 %), primarily due to the side-wall roughness. The roughness resulted in a larger perimeter measurement (33.3–75%). However, there is a noticeable discrepancy in RH3. This channel array is an example where residual wax can remain within the side-wall reducing both CSA and perimeter. This is a shortcoming of the cleaning technique as it cannot consistently remove all wax from the channels due to the pronounced side-wall roughness. This also highlights an issue with scale when designing horizontally printed channels: i.e., at larger channel scales, the side-wall roughness will have a reduced effect on channel characteristics.

Table 4 is a comparison of the measured channel heights and widths with the nominal dimensions. This table also contains the variation of heights and widths for each microchannel array.

The measured rectangular channel heights have a lower variance than the measured widths. The reason for such high variance in width is the side-wall roughness which makes it difficult to discern the characteristic width of the channels. The width measurements presented here are measured from the base of each side-wall. The deviations from the nominal dimensions vary in both height and width. The rectangular channels, RH1 & RH2, are greater than the nominal height, while the widths are less than the nominal. A reason for this bias is the side-wall

Table 3. Comparison of the nominal and measured channel CSAs (mm^2) and perimeter (mm) for the horizontal 3D-printed channels. Channel-to-channel variance per array and percentage deviation from the nominal dimension are presented.

	Nominal		Measured		Variance (%)		Change (%)	
Channel Type	CSA	Perimeter	CSA	Perimeter	CSA	Perimeter	CSA	Perimeter
RH1	0.101	1.20	0.110	2.10	9.3	21.7	8.9	75.0
RH2	0.101	1.20	0.113	2.10	9.6	14.6	11.9	75.0
RH3	0.101	1.20	0.069	1.18	15.7	27.1	-31.7	-1.6
TH1	0.123	1.50	0.125	2.00	15.2	20.4	1.6	33.3
TH2	0.123	1.50	0.121	2.30	5.5	20.1	-1.6	53.3
TH3	0.123	1.50	0.121	2.30	9.7	19.3	-1.6	52.6

Table 4. Comparison of the nominal and measured channel dimensions for the horizontal channels. Channel-to-channel variance per array and percentage deviation from the nominal dimensions are presented.

	Nominal (mm)		Measured (mm)		Change %		Variance %	
Channel Type	Height	Width	Height	Width	Height	Width	Height	Width
RH1	0.304	0.332	0.358	0.282	17.6	-15.2	6.6	19.3
RH2	0.304	0.332	0.364	0.259	19.7	-22.1	6.2	11.7
RH3	0.304	0.332	0.303	0.237	-0.4	-28.6	4.2	10.9
TH1	0.413	0.577	0.439	0.468	6.3	-18.8	10.3	16.1
TH2	0.413	0.577	0.420	0.472	1.8	-18.1	13.6	18.7
TH3	0.413	0.577	0.412	0.491	-0.4	-14.9	16.5	7.1

roughness present in the channels. The measured trapezoidal channel heights were close to that to the nominal dimension (0.4–6.3 %). This result is due to the bowing feature present in the trapezoidal channel, which compensates for loss of the base width (21 μm). Although horizontal printing embedded channels yields good design flexibility, the degree of shape conformity and dimensional fidelity associated with the printing process are poor in comparison to both Silicon and vertical channels; as a result, this technique does not lend itself to creating dimensionally accurate channels. Similar to the vertical printing method, larger scale channels may yield higher dimensional accuracy as the side-wall roughness would have a diminishing effect on channel characteristics.

4.3. Surface profiles

This section compares the surface characteristics of the vertically and horizontally printed microchannel arrays fabricated and in order to determine effect of surface roughness along the channel length. To this end, SEM imaging of the exposed channel types, complemented with surface profiles, are presented. Finally, a spectral analysis of the surface profile plot was performed to detect the presence of spatially periodic roughness features along the channel length. Figure 5 illustrates the surface characteristics for both rectangular and trapezoidal vertical microchannel arrays with SEM images, sample profilometry measurements and a histogram of the distribution of profile height along the channel length.

Visual inspection of the rectangular channel profile, figure 5(a), shows a rough surface. The

profile measurement of the channel length shows no clear periodic features, however a spectral analysis revealed a strong feature to be present every 200 μm along the channel length. The surface profile shows that the maximum feature size ranges between $\pm$20 μm, which is close to the printer resolution of $\pm$16 μm. The side-wall appears to be perpendicular to the base wall which implies a rectangular cross-section is maintained along the channel length. Finally, the side-wall roughness along the channel length appears to be similar to the base wall throughout the channel length, which implies a uniform roughness and surface profile along the channel length. Figure 5(b) shows the SEM image of the exposed trapezoidal channel accompanied with a surface profile and histogram of the same surface profile. Roughness features were found to be present at the base and side-wall of the trapezoidal channel. The resolution of the base width feature of 21 μm is lost with the average measurement being visually larger that the nominal value (approx. 100 μm). There are significant steps changes along the trapezoidal walls which suggests that the angled walls are not smooth. The metrology of the trapezoidal channel highlights the limit of the printer in creating embedded trapezoidal or triangular features. The surface profile shows no clear periodic features and is only presented up to 3 mm. This is due to the probe moving up the side-wall. It is important to note that adjusting the probe alignment correctly within the channel is difficult as the tolerances are small (approx. $\pm$50 μm). As a result, the histogram plot only uses data taken up to this point to prevent skewing of the distribution. A spectral analysis revealed two strong peaks occur at every 250 μm and 500 μm along the channel length. The histogram plot shows that the change in surface profile height is approximately $\pm$16 μm. Overall, the surface profile measurements for each vertical channel shape are approximately the resolution of the printer.

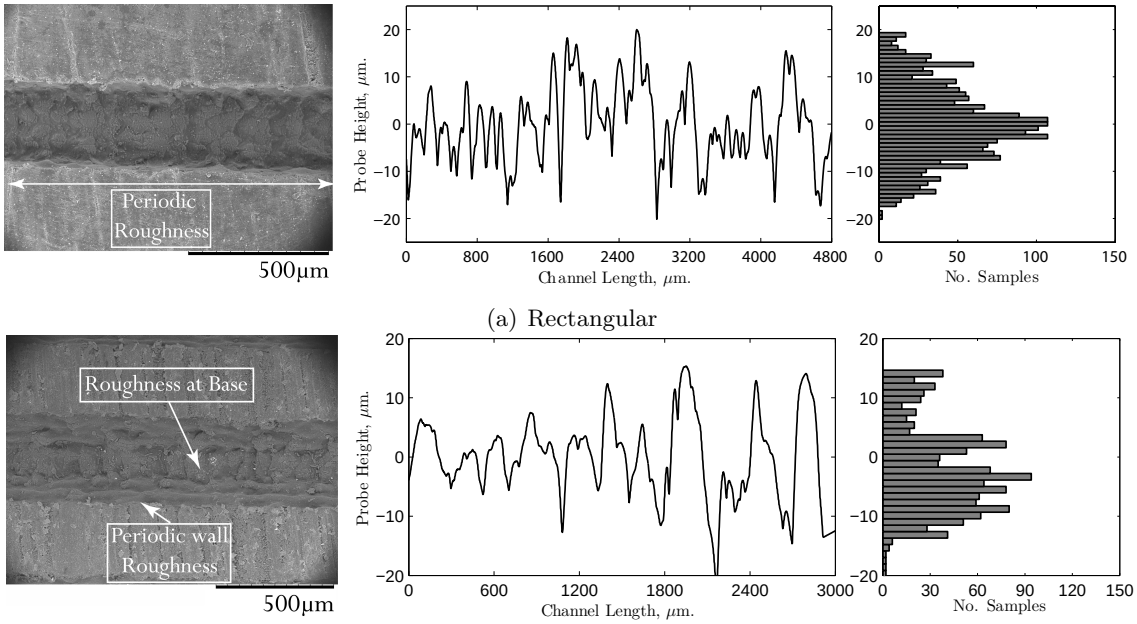

Figure 5. SEM images of the vertical channel designs with their respective surface profile measurements and related statistics.

Figure 6 depicts SEM images of the exposed horizontal 3D-printed microchannel arrays complete with both a sample surface profile measurement and histogram plot. A spectral anaylsis of the profile was carried out to determine if there were any periodic features present along the channel.

Figure 6(a) shows the exposed channel and surface profile information along the channel

length. The SEM imaging shows a strong patterned feature along the channel length. The pattern produced in the horizontal rectangular microchannel array is more consistent than that of the vertical rectangular microchannel arrays. The surface profile measurement shows no evident pattern, however the spectral plot revealed periods every 150 and 300 μm. The histogram plot revealed the change in profile height to be within ± 10 μm which is within the printer's highest resolution limit (± 16 μm)and performs better than the vertically printed channel. The side-wall roughness which was highlighted in the channel cross-section is evident along the channel sides due to protrusions from the side-wall.

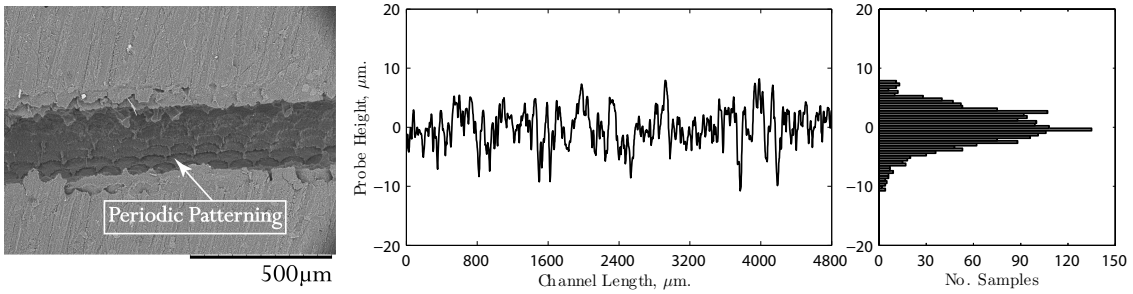

(a) Rectangular

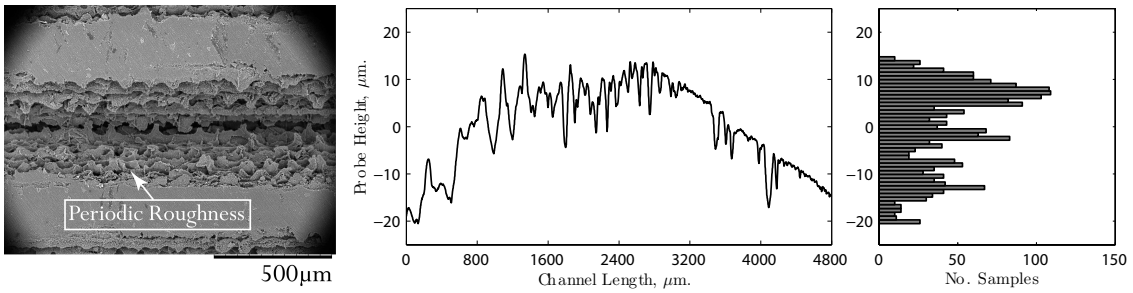

(b) Trapezoidal

Figure 6. SEM images of the horizontal channel designs with their respective surface profile measurements and related statistics.

Figure 6(b) shows the exposed horizontal trapezoidal microchannel, and depicts extensive side-wall roughness. Periodic patterning is evident along the channel length, however it is not as clear as the horizontal rectangular channel (Figure 6(a)). The surface profile depicted is not entirely representative of the total surface roughness of the channel. This is due to the coupled effect of the side-wall roughness and trapezoidal shape of the channel, as the probe was possibly travelling between the side-wall roughness layers along the channel length. This yields a visible bias in the histogram profile. Overall, the roughness present in the trapezoidal channel is extensively greater than the other channel measured and is not within the printer resolution. A spectral analysis of the profile revealed no periodic features present along the channel length.

The surface profile analysis shows that the profile along the channel length was approximately the resolution of the printer for the vertical channel. This is important when fabricating microchannels via vertical 3D-printing as this is the minimum roughness that will be present in the channels. At larger channel scales, the effect of surface roughness will be diminished: for example, a channel of 1000 μm hydraulic diameter would have a roughness of 3.2 % of the diameter for the given printer resolution. The horizontal channel featured a significant differing surface roughness features, with the side-wall present larger roughness than the base-wall. The trapezoidal channel surface profile presents a complex profile which is due to the side-wall roughness feature. Again, printing at a larger scale will diminish the side-wall roughness on embedded horizontally printed channels. Although the vertical printing approach yielded superior quality channels than the horizontal approach, printing vertically has more

design constraints than horizontally printing, in particular that no overhanging feature can be incorporated into the design. This should be taken into consideration when fabricating embedded microchannel arrays. The paper highlights the capabilities of 3D-printing embedded microchannels; however, a comprehensive error analysis is needed to fully quantify the impact surface roughness has on channel characteristics.

5. Conclusions

A direct dimensional comparison between Silicon and equivalent 3D-printed microchannel arrays was conducted which considered the dimensional fidelity and shape conformity of the arrays. The following was concluded:

- The Silicon microchannel arrays produced superior quality channels compared to the 3D-printed equivalent. The vertical 3D-printed channel produced good shape conformity and lends itself to microchannel manufacture when compared to the horizontal printing approach.
- The CSA of the vertical channels were consistently less than the nominal dimensions due to curvature present at corners. This feature was a function of material shrinkage during the printing process and should be accounted for in its design.
- The horizontal channels demonstrated inferior shape conformity which was due to the additional side-wall roughness. This feature reduces the quality of the channel produced but would have a reduced effect for channels printed of larger scale.
- The surface profile varied about the resolution of the printer for the vertical 3D-printed channels (approx. 16 μm), however the surface roughness produced by the horizontal channels was larger than the printer resolution. Printing at larger scales would reduce this effect. A spectral analysis revealed a spatial surface periodicity along the vertical printed channels and horizontal printed rectangular channels. No notable patterns were evident in the horizontally printed trapezoidal channel.

In summary, for microfluidics research, vertically 3D-printed microchannels can yield suitable shape conformity and dimensional fidelity with variances two to four times larger than conventional fabrication techniques such as DRIE and wet-etching.Dimensional characterization is an important parameter as the variances measured with all fabrication methods can have direct implications on the hydrodynamic performance due to its sensitivity to channel dimensions.

Acknowledgments

The authors acknowledge the financial support of Science Foundation Ireland (SFI) under grant number 10/CE/I1853. Bell Labs Ireland would like to thank the Industrial Development Agency (IDA) Ireland for their continued support.

References

[1] Agostini B, Fabbri M, Park J E, Wojtan L, Thome J, R, and Michel B 2007 *Heat Transfer Eng.* **28** 4 p 258
[2] Eason C, Dalton T, Davies M, O'Mathna C, and Slattery O 2005 *Heat Transfer Eng.* **26** 3 p 79
[3] Martynova L, Locascio L E, Gaitan M, Kramer G W, Christensen R G, MacCrehan W A 1997 *Anal. Chem.* **69** 23 p 4783
[4] Paydar O H, Paredes C N, Hwang Y, Paz J, Shah N B, Candler R N 2014 *Sensor. Actuat. A-Phys.* **205** 0 p 199
[5] McDonald J C, Chabinyc M L, Metallo S J, Anderson J R, Stroock A D and Whitesides G M 2002 *Anal. Chem.* **74** 7 p 1537
[6] Moore J L, McCuiston A, Mittendorf I, Ottway R, and Johnson R D 2010 *Microfluid. Nanofluid.* **10** 4 p 877
[7] Bonyár A, Sántha H, Ring B, Varga M, Gábor Kovács J, Harsányi G 2010 *Procedia Engineering* **5** p 291
[8] Krejcova L, Nejdl L, Rodrigo M, Angel M, Zurek M, Matousek M, Hynek D, Zitka O, Kopel P, Adam V, and Kizek R 2013 *Biosens. Bioelectron.* **54** p 421
[9] McCullough E J and Yadavalli V K 2013 *J. Mater. Process Technol.* **213** 6 p 947
[10] Steinke M E and Kandlikar S G 2006 *Int. J. Therm. Sci.* **45** p 1073
[11] Wang R J, Wang L, Zhao L, and Liu Z, 2007 *Int. J. Adv. Manuf. Technol.* p498-504